IEEE Access
Multidisciplinary | Rapid Review | Open Access Journal

SPECIAL SECTION ON UNDERWATER WIRELESS COMMUNICATIONS AND NETWORKING

Received December 15, 2017, accepted January 29, 2018, date of publication March 12, 2018, date of current version April 23, 2018.

Digital Object Identifier 10.1109/ACCESS.2018.2815026

A High-Rate Software-Defined Underwater Acoustic Modem With Real-Time Adaptation Capabilities

EMRECAN DEMIRORS[1], (Member, IEEE), GEORGE SKLIVANITIS[2], (Member, IEEE), G. ENRICO SANTAGATI[1], (Student Member, IEEE), TOMMASO MELODIA[1], (Fellow, IEEE), AND STELLA N. BATALAMA[3], (Senior Member, IEEE)

[1]Department of Electrical and Computer Engineering, Northeastern University, Boston, MA 02115, USA
[2]Department of Computer and Electrical Engineering and Computer Science, Florida Atlantic University, Boca Raton, FL 33431-0991, USA
[3]College of Engineering and Computer Science, Florida Atlantic University, Boca Raton, FL 33431-0991, USA

Corresponding author: Emrecan Demirors (edemirors@ece.neu.edu)

This work was supported by the National Science Foundation under Grant CNS-1503609 and Grant CNS-1726512.

ABSTRACT There is an emerging need for high-rate underwater acoustic (UW-A) communication platforms to enable a new generation of underwater monitoring applications including video streaming. At the same time, modern UW-A communication architectures need to be flexible to adapt and optimize their communication parameters in real time based on the environmental conditions. Existing UW-A modems are limited in terms of achievable data rates and ability to adapt the protocol stack in real time. To overcome this limitation, we present the design, implementation, and experimental evaluation of a new high-rate software-defined acoustic modem (SDAM) with real-time adaptation capabilities for UW-A communications. We introduce new physical-layer adaptation mechanisms that enable either joint adaptation of communication parameters such as modulation constellation and channel coding rate or seamless switching between different communication technologies such as orthogonal-frequency-division-multiplexing and direct-sequence-spread-spectrum. The performance of the proposed SDAM has been evaluated in both indoor (water tank) and outdoor (lake) environments. We demonstrated that the SDAM achieves 104 kbit/s with bit-error-rate (BER) of 2×10^{-5}, 208 kbit/s with BER of 10^{-3}, and 260 kbit/s with BER of 10^{-2} in real time over a 200 m horizontal link at a very-shallow lake environment.

INDEX TERMS Underwater acoustic networks, underwater acoustic communication, high date rate, real-time video streaming, reconfigurability, real-time adaptation, software-defined acoustic modem.

I. INTRODUCTION

Underwater acoustic (UW-A) wireless communications and networking is today a key technology in many military, commercial, and scientific applications, including tactical surveillance, offshore exploration, monitoring of subsea machinery (e.g., oil-rigs, pipelines), disaster prevention, climate change prediction, pollution control and tracking, and study of marine life [2]. While UW-A networks are receiving increasing attention, application requirements and needs are at the same time becoming increasingly demanding. Applications such as deep-water oil-rig supervisory monitoring already require real-time streaming capability of non-static images between wireless underwater nodes (e.g., Unmanned Underwater Vehicles (UUV), divers).

To address this need, underwater links are required to support sufficiently high data rates, compatible with the streaming rates of the transmitted video sequence. Unfortunately, the *temporal* and *spatial* variations of the UW-A channel due to high path loss, time-varying multipath propagation, high and variable propagation delay, and Doppler spread [2], limit the available bandwidth and consequently the achievable data rates. Thus, UW-A communication systems need to be flexible and capable of adapting their communication parameters in real time based on the environmental conditions to guarantee connectivity and maximum performance at all times.

Yet, most commercially available acoustic modems rely on fixed hardware designs and proprietary protocol solutions

and achieve data rates lower than 35 kbit/s [3]–[6]. Recently, a commercially available modem has been advertised to support transmission rates of 62.5 kbit/s over a 300 m underwater link [7], which may adequately satisfy the demands of specific applications. However, the above data rates may not be sufficient to support real-time video streaming and, at the same time, the non-flexible nature of the modem design [7] does not allow system adaptation in real time based on space- and time-varying channel and interference conditions. Consequently, there is a clear need for new UW-A communication platforms that can (i) support data rates to stream video and (ii) intelligently decide and adapt their communication parameters based on the environmental conditions in real time.

In the radio-frequency (RF) wireless domain, software-defined radios (SDRs) have, in recent years, taken a key role in enabling intelligently adaptive and reconfigurable systems that are able to accommodate and rapidly test novel communication protocols [8]–[13]. The unique features and capabilities of SDR may play a pivotal role in the effectiveness of UW-A communications and make SDR-based devices a particularly promising solution for UW-A communications. Previous work [14]–[17] has predicted the potential benefits of a possible paradigm shift of the design of UW-A communication devices from hardware-based to SDR-based.

In this article, we introduce a custom, high-rate, highly reconfigurable software-defined acoustic modem (SDAM) for UW-A communications. The architecture of the SDAM is built around a commercial SDR interfaced with a wide-band acoustic hydrophone through custom amplifying circuitry. The proposed SDAM offers (i) higher data rates compared to existing commercial and experimental acoustic modems and (ii) capability of reconfiguring its physical layer in real time under rapidly varying environmental conditions. The prototype SDAM is based on a Universal Software Radio Peripheral (USRP N210) interfaced with a Teledyne RESON TC4013 miniature wideband hydrophone that is used both for projecting and receiving sound in a time division fashion. The software-defined functionalities at the physical and link layers of the SDAM are implemented mainly in GNU Radio and are executed on a host-PC. At the physical layer, the proposed SDAM considers a high-rate zero-padded orthogonal-frequency-division-multiplexing (ZP-OFDM) scheme for the forward link and a robust, low rate binary chirp spread-spectrum modulation (B-CSS) scheme for the feedback (receiver to sender) link. Additionally, the proposed SDAM implements at the physical-layer, novel, real-time reconfiguration mechanisms that enable either joint adaptation of several communication parameters of a pre-selected communication technology such as modulation constellation and channel coding rate or seamless switching between different communication technologies such as ZP-OFDM and direct-sequence spread spectrum (DS-SS) to effectively adapt to channel conditions and application requirements.

We deployed and tested custom-built SDAMs in both indoor (water tank) and outdoor (lake) environments. First, we evaluated the proposed system setup in terms of bit-error-rate (BER) as a function of signal-to-interference-plus-noise-ratio (SINR) at the receiver, for various modulation schemes and error-correction coding rates. Second, we demonstrated real-time adaptation of the modulation and error-correction coding rate in the ZP-OFDM forward link to solve a rate maximization problem under pre-defined BER reliability constraints. Third, we demonstrated for the first time seamless runtime handoff on an operational acoustic link between ZP-OFDM and DS-SS communication technologies. Finally, we demonstrated, for the first time to the best of our knowledge, that the proposed SDAM can achieve real-time data rates up to 260 kbit/s over a 200 m horizontal link in shallow water.

To summarize, the major contributions of this paper are:

- Design and deployment of a high-rate, highly reconfigurable software-defined acoustic modem
- Design and implementation of a new robust chirp-based feedback channel
- Design and implementation of adaptation mechanisms that enable real-time adaptation of PHY layer communication parameters (e.g., modulation, error-correction coding rate) and seamless switching between different communication technologies
- Design, implementation, and real-time demonstration of an OFDM scheme that achieves data rates up to 260 kbit/s over a 200 m horizontal link in shallow water

The rest of the paper is organized as follows. In Section II, we review related work and present the current state of the art. In Section III, we describe the proposed modem architecture and discuss the design and synthesis of a software-defined underwater acoustic modem from first principles. In Section IV, we discuss the physical layer schemes for the forward and feedback communication links. In Section V, we present performance evaluation results from experiments/deployments conducted in both indoor (water test tank) and outdoor (lake) underwater environments. Finally, a few concluding remarks are provided in Section VI.

II. RELATED WORK

In this section, we review the current state of the art in commercial underwater acoustic modems and related experimental work, particularly in terms of achievable data rates and adaptation capabilities in an effort to establish benchmarks for the proposed SDAM.

A. COMMERCIAL ACOUSTIC MODEMS

1) ACHIEVABLE DATA RATES

There are a handful of companies that offer commercial underwater acoustic modems that support different data rates for different ranges. DSPComm offers an underwater wireless modem called AquaComm [3]. AquaComm is able to achieve a data rate of 480 bit/s over a 3 km underwater link. AquaSent AM-OFDM-13A [4] is an underwater acoustic modem that has a communication range of 5 km and a maximum data

rate of 9 kbit/s. Teledyne Benthos [5], a leading manufacturer of underwater acoustic equipment in the United States, offers a wide range of acoustic modems that incorporate proprietary phase shift keying (PSK) and M-ary frequency shift keying (MFSK) transmission schemes supporting data rates up to 15 kbit/s over 2–6km underwater links. LinkQuest UWM2200 [6] is another wireless underwater modem that can support a maximum data rate of 38 kbit/s up to a range of 1 km. Because of the physical characteristics of the underwater acoustic channel [2], only acoustic/ultrasonic waves at low frequencies (e.g., less than 50 kHz) can propagate over *km*-range distances. Therefore, commercial modems generate acoustic waves through low-frequency piezoelectric resonators, which inevitably have limited bandwidth (i.e., in the order of a few kHz). However, when transmitting over shorter distances, as in many sensing and control applications of interest, for example, to oil and gas and fishing industries, among others, it would be desirable to use wider bandwidths in the ultrasonic regime (> 50 kHz) and generate wideband multicarrier waveforms to communicate at higher data rates. As of today, EvoLogics S2CM-HS [7] is the only commercial modem, to the best of our knowledge, that is reported to use a frequency band of $120 - 180$ kHz to support a maximum data rate of 62.5 kbit/s over a range of 300 m.

2) ADAPTATION CAPABILITY

Commercially available underwater acoustic modems are typically based on fixed hardware solutions that incorporate proprietary protocols. As a consequence, they support either no or very limited adaptation capabilities. In fact, most prior work [18]–[20] that focuses on adaptive physical layer schemes considers UW-A modems that offer a limited number of operating modes and data recording capabilities. Adaptation to environmental variations is driven by/decided upon extensive offline simulations and it is merely a switch among a small, fixed number of operational modes. The work in [21] discusses design considerations and presents experimental results of an adaptive OFDM scheme. The designed scheme was implemented using off-the-shelf acoustic modems that can perform adaptation by switching between a set of predefined operational modes (pre-fixed set of communication parameter values). In summary, while existing solutions may satisfy the requirements of specific application scenarios, they lack (i) the capability of switching between the operational modes in real time, (ii) algorithmic and architectural support for decision making, and (iii) the ability to intelligently adapt to all possible environmental conditions due to the finite number of operational modes.

B. EXPERIMENTAL ACOUSTIC MODEMS AND RESEARCH ACTIVITIES

1) ACHIEVABLE DATA RATES

Current experimental acoustic modems and research activities typically focus on signaling schemes and modem architectures either for low data rate (i.e., 20 kbit/s) over medium-range links (i.e., $1 - 10$ km) or relatively higher data rate (i.e., $\sim$ 100 kbit/s) over very short-range links (i.e., > 20 m). Micro-Modem [22], which is developed at the Woods Hole Oceanographic Institute (WHOI), is one such experimental modem that can achieve data rates from 80 bit/s to 5.3 kbit/s at a communication range of $2 - 4$ km. On the other hand, experimental results obtained by processing of collected data in [23] report a data rate of 48 kbit/s at a 2 km range, when four (4) transmitters incorporate space-time coding techniques. The work in [24] describes an experimental software-defined acoustic modem that performs data transmission at a rate of 80 kbit/s over a 15 m very-short range underwater link. The work in [25] reports data rates as high as 150 kbit/s, but only on very short (15 m) vertical links, which are not affected by multipath. Finally, the work in [26] presents data rates of 522 kbit/s obtained over short horizontal links (e.g., 10 m).

2) ADAPTATION CAPABILITY

Several recent papers have focused on the development of new experimental modems which can support adaptation through partially or fully software-defined protocol implementations. For example, [27] presented an underwater acoustic networking platform based on the USRP platform that exploits open-source software tools (GNU Radio, TinyOS, and TOSSIM) to implement physical and data-link layer functionalities with parameter adaptation capability. Similarly [14], [24], and [28] proposed modem designs that are based on FPGA/DSP or FPGA-only cores. These architectures provide support for software-defined physical and data-link layers that offer real-time parameter adaptation. The work in [29] presents a reprogrammable modem design that is built on a general-purpose computing architecture with open-source operating systems and tools. In [30], adaptation at multiple layers is discussed for a new low-power and low-cost platform based on a general-purpose processor which supports software-defined functionalities that span physical, data-link, network, and application layer.

III. SDAM ARCHITECTURE

The custom SDR-based acoustic modem proposed in this paper consists of (i) a USRP N210, (ii) a host-PC, (iii) a power amplifier and a voltage preamplifier, (iv) an electronic switch, and (v) a wideband acoustic (ultrasonic) hydrophone. The hardware architecture of the proposed modem is illustrated in Fig. 1, while the SDAM prototype is depicted in Fig. 2.

A. USRP N210

The proposed architecture is based on USRP N210, a commercially available, FPGA-based, SDR platform that offers a wide range of radio front-ends through interchangeable daughterboards that cover the frequency spectrum from DC to 5 GHz. We selected LFTX and LFRX daughterboards ($\text{DC} - 30$ MHz), which enable the development of a half-duplex transceiver operating in the frequency range of the selected acoustic transducer

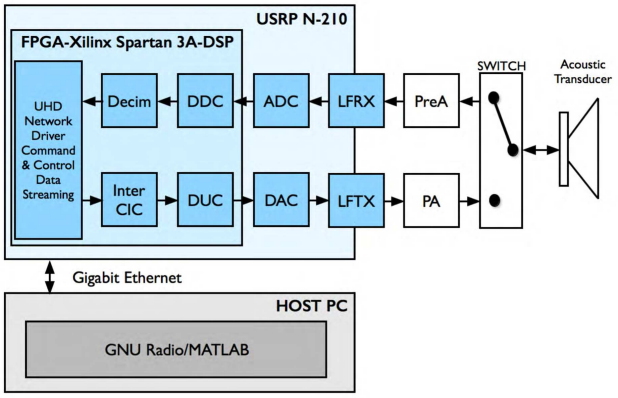

FIGURE 1. Hardware architecture of the software-defined acoustic modem (SDAM).

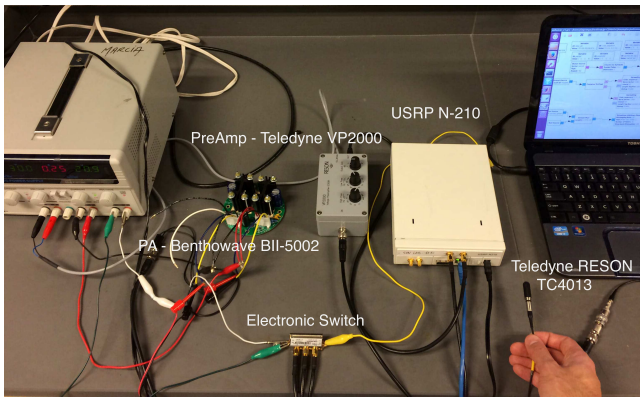

FIGURE 2. The proposed SDAM prototype.

(1 Hz – 170 kHz). The USRP motherboard is equipped with a (dual 100 MSample/s, 14-bit) analog-to-digital converter (ADC) and a (dual 400 MSample/s, 16-bit) digital-to-analog-converter (DAC) that are both controlled by a 100 MHz master clock. The sampling rate of the incoming digital samples (from the ADC) and outgoing samples (to the DAC) is fixed at 100 MSample/s. The FPGA digitally interpolates/decimates the stream to match the hardware sampling rate to the rate requested by the user. High rate baseband signal processing can be conducted either directly in the FPGA (Xilinx Spartan 3A-DSP3400) or in the host-PC, which is connected to the SDR through Gigabit Ethernet (GigE).

Transmitter/receiver algorithms and data-link control protocols are implemented in the open-source software framework called GNU Radio, which is commonly used to drive the USRP from a host-PC, as well as to implement signal processing operations (possibly in combination with the MATLAB scripting language). GNU Radio offers a broad set of signal processing blocks implemented in C++ that can be used to develop a large variety of wireless communications applications. These C++ blocks are usually wrapped into Python classes and are either instantiated from Python scripts, or used as building blocks of a communication flowgraph from a graphical user interface. We selected GNU Radio not only because of its library available communication building blocks that allow rapid prototyping of PHY layer schemes, but also because of its capability to easily create new custom signal processing blocks and thus create customized transceiver designs. Both forward and feedback links discussed in this paper are implemented using GNU Radio blocks. Some of the receiver functionalities combine both GNU Radio blocks and MATLAB scripting language.

The sample rate and, accordingly, the bandwidth of our implementation is bounded primarily by two factors [9]. First, the GigE connection between the host-PC and the USRP can support sample rates up to 25 MSample/s. If the host sample rate is exceeded, then the GigE connection experiences network packet drops that causes loss of digital samples. Second, the software implementation of certain digital signal processing blocks (in GNU Radio) as well as the inter-process communication between PHY layer blocks and data-link control protocols introduce processing latency [8], [12], [31], which limits the host sample rate. Thus, if the host-PC is not capable of processing the incoming/outgoing data samples as fast as the user-requested sample rate, the GNU Radio buffers overflow/underflow and thus digital samples are lost. The sample rate requirements of our implementation are satisfied by a fully software implementation in GNU Radio and MATLAB.

B. POWER AMPLIFIER, VOLTAGE PREAMPLIFIER, AND SWITCH

To enhance the communication range of our system, we selected a commercial off-the-shelf linear wideband power amplifier (PA), Benthowave BII − 5002. The PA has maximum output power of 192 dB, and can support up to 300kHz bandwidth. It is used for amplifying the output power of the LFTX daughterboard (i.e., 2 mW) and accordingly provides a maximum transmission power of 1 W. Half-duplex operation between TX / RX with a single acoustic transducer is achieved through a commercial electronic switch, Mini-Circuits ZX80 − DR230+. The latter guarantees low insertion loss and very high isolation over the frequency range of 0 − 3 GHz. The switch is controlled through the General Purpose Input/Output (GPIO) digital pins available on the LFTX and LFRX daughterboards. At the receiver side of the switch, we connect a voltage preamplifier (PreA), Teledyne RESON VP2000, which provides low-noise performance in the desired frequency range with a range of bandpass filters, and adjustable gain selection.

C. ACOUSTIC TRANSDUCERS

We used TC4013 acoustic transducers (receiver hydrophones) manufactured by Teledyne RESON, which offer an operational frequency range from 1 Hz to 170 kHz. These transducers were selected mainly because of the relatively wide frequency bands that they can support, which allow high data rate communications and enable the implementation of a variety of physical layer schemes. TC4013s provide receiving sensitivity of −211 [dB re 1V /μPa at 1 m] that is relatively

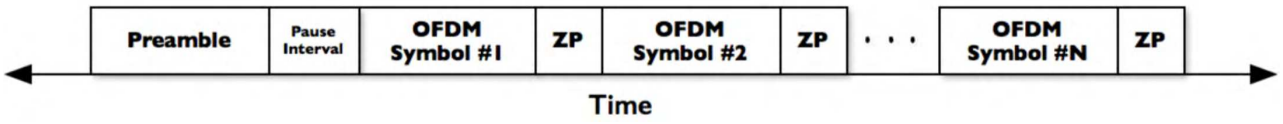

FIGURE 3. Packet format of the ZP-OFDM scheme.

flat over the operational frequency range and transmitting sensitivity of 130 [dB re 1μPa/V at 1 m] at 100 kHz. The acoustic transducers used in the proposed SDAM prototype have omnidirectional horizontal and 270° vertical directivity patterns.

IV. PHYSICAL LAYER ADAPTATION

In this section, we describe the developed mechanisms for real-time adaptation of the PHY layer parameters and for switching in real time between alternative signaling schemes supported by the proposed modem. A chirp-based feedback link is also defined to provide a reliable, low data rate method for updating the transmitter parameters and switching seamlessly between different communication technologies upon a decision taken at the receiver.

OFDM PHY. Phase-coherent OFDM schemes have been used extensively in UW-A communications because of their robustness against frequency selective channels with long delay spreads [20], [30], [32]. In this paper, we designed a custom zero-padded (ZP) OFDM scheme, where each OFDM symbol is followed by padded zeros as illustrated in Fig. 3. We chose a zero-padding scheme over other alternatives such as cyclic prefixing (CP), primarily because of its energy efficiency. More specifically, each transmission packet is designed to have N ZP-OFDM symbols over K subcarriers. Each subcarrier is designated either as data, pilot, or null subcarrier. Data subcarriers are used to allocate data symbols. Data symbols are modulated versions of information bits, and are coded with a convolutional error-correction coding scheme, and different gray-coded modulation schemes (e.g., binary-phase-shift-keying (BPSK), quadrature-phase-shift-keying (QPSK), 4 quadrature-amplitude-modulation (4-QAM), 8-PSK, 8-QAM, 16-QAM, 32-QAM). Pilot subcarriers are allocated to pilot symbols (symbols known to both the transmitter and the receiver) and are used for channel estimation and symbol-level (fine) synchronization. Pilot and null subcarriers are used for Doppler scale estimation. The signaling scheme introduces a guard interval between each OFDM symbol to avoid inter-symbol-interference (ISI). The proposed system uses a preamble based on a pseudorandom noise (PN) sequence that precedes each packet and is used for packet detection and coarse synchronization.

Figure 4 depicts a block-level representation of the GNU Radio flowgraph that implements the proposed ZP-OFDM transmitter. First, information bits are relayed from the data-link layer to the flowgraph through a data FIFO, which is

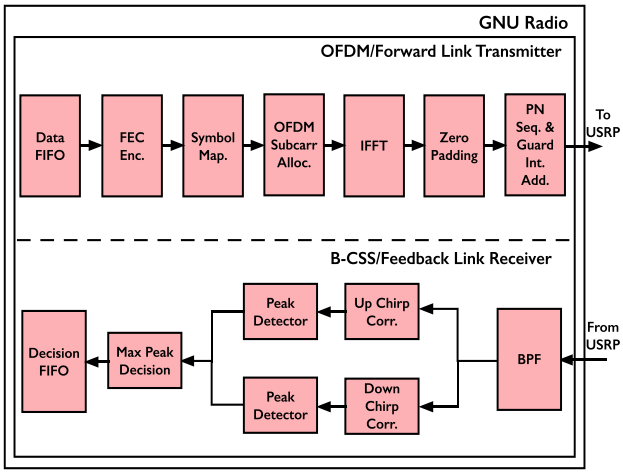

FIGURE 4. Block diagram of the ZP-OFDM transmitter and B-CSS receiver.

controlled by a Python thread. The input information bits are encoded through a forward-error-correction (FEC) encoder (i.e., convolutional encoder) and later mapped into symbols according to the selected modulation scheme. The symbols generated are then allocated to different data subcarriers alongside with pilot and null subcarriers based on a predefined scheme to form the OFDM symbols. We denote as $K_P = K/4$, K_D, and K_N the number of pilot, data and null subcarriers, where K represents the total number of subcarriers. The ZP-OFDM symbols are obtained through an IFFT operation on each OFDM symbol and appropriate zero padding. The generated ZP-OFDM symbols are then converted into a packet, where a preamble and guard intervals are inserted to form the packet structure depicted in Fig. 3. All transmitter functionalities are implemented in GNU Radio either by defining new or by customizing already available communication building blocks.

On the receiver side (Fig. 5) a low-pass filter (LPF) is first used to eliminate out-of-band noise and interference. Incoming data are then pushed into a FIFO queue that is continuously polled by a MATLAB process thread. The correlation properties of the PN sequence in the transmitted packet are leveraged to detect the beginning of the ZP-OFDM packet and perform receiver synchronization. Each ZP-OFDM packet is then partitioned into individual OFDM symbols. On each OFDM symbol, we carry out pilot-tone based symbol synchronization [32], Doppler scale estimation and compensation based on pilot and null subcarriers [32], input SINR evaluation [21], pilot-tone

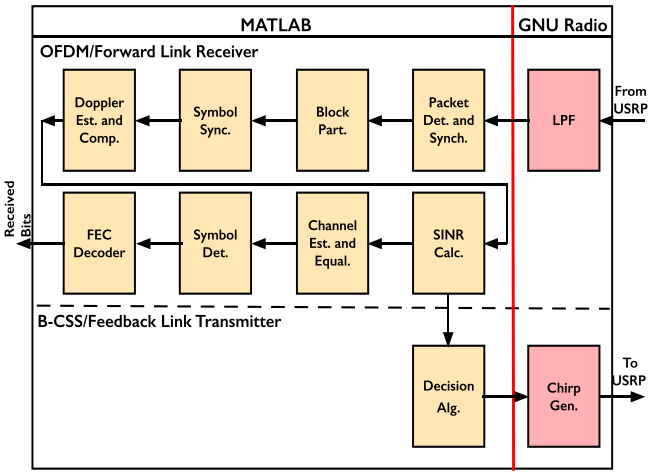

FIGURE 5. Block diagram of the ZP-OFDM receiver and B-CSS transmitter.

based channel estimation [33], zero-forcing (ZF) channel equalization, and symbol detection. Finally, the received bits are acquired by decoding with the corresponding FEC decoder. The receiver architecture is based on a hybrid MATLAB/GNU Radio implementation.

A. OFDM PHY ADAPTATION

The decision/adaptation mechanism is driven by the receiver, which estimates the input SINR and selects the optimal transmission strategy to satisfy a pre-defined BER threshold (BER_{th}). Formally, the PHY decision algorithm solves the following maximization problem

$$\underset{M,C}{\text{maximize}}\ R(M, C) \tag{1}$$

$$\text{subject to}\ BER_{\text{th}} \geq BER(SINR, M, C), \tag{2}$$

where R denotes the data rate that is a function of the modulation order M and the error-correction coding rate C. BER is a function of M, C and the $SINR$ estimated at the receiver. BER_{th} denotes a pre-defined BER reliability threshold. The data rate R is defined as

$$R(M, C) = \frac{K_D C log_2(M)}{T_s + T_g}, \tag{3}$$

where K_D is the number of data subcarriers, T_s is the OFDM symbol duration, and T_g is the duration of the guard interval. In Section V, we will discuss how the parameters M and C are selected for fixed K_D, T_s and T_g to maximize the data rate under pre-defined BER reliability constraints.

The rate maximization problem in (1) is solved in a decision algorithm block implemented and executed in MATLAB. The rate-maximizing values of M and C are then sent to the GNU Radio flowgraph that implements the feedback transmission link (Fig. 5). The optimal strategy decided by the receiver is fed back to the transmitter node through a robust chirp-based underwater wireless feedback link. After successfully decoding the feedback message, the transmitter synchronizes with the decision taken at the receiver and adopts the optimal encoding strategy selected at the receiver for its next data packet transmission. Parameter adaptation at the transmitter side is performed via a Python thread that controls the convolutional encoder, the symbol mapping, and the subcarrier allocation blocks of the transmitter GNU Radio flowgraph.

In the rare case of a lost feedback frame, the transmitter and the receiver become unsynchronized in terms of their encoding strategy. As a result, received frames with errors are discarded. Both transmitter and receiver will be synchronized to a new encoding strategy upon successful delivery of a new feedback frame. The design of throughput efficient forward/feedback-link strategies that minimize the number of dropped packets in both forward and feedback links is out of the scope of this paper.

B. SWITCHING BETWEEN DIFFERENT SIGNALING SCHEMES

To demonstrate switching between different communication technologies, we have also implemented DS-SS transmitter/receiver flowgraphs by developing custom communication blocks in GNU Radio. Each transmission frame consists of P unmodulated pilot symbols in $\{1\}$ and N data bits that are mapped to $\{\pm 1\}$ BPSK modulated symbols. Each symbol is then spread in L chips through a custom built block that outputs $(N + P)L$ chips in $\{\pm 1\}$. A RAKE receiver is implemented in GNU Radio and pilot symbols are used for frame detection, channel estimation, and symbol synchronization [34]. The decision mechanism adopted for this scenario is based on successful decoding of an incoming packet. More specifically, both OFDM and DS-SS flowgraph instances are defined in the SDAMs and their operation is controlled by a multiplexer block implemented in GNU Radio. The enabling signal for this multiplexer is controlled by a boolean variable that enables DS-SS transmission/reception upon successful reception of an OFDM packet and vice versa. The feedback link in this case is used as the carrier of the multiplexer-control signal that enables the seamless switch between the two communication technologies at the transmitter. The ability of the proposed modems to support hybrid communication technologies is of significant importance and will play a key role in future deployments of "cognitive" underwater acoustic networks.

C. CHIRP-BASED FEEDBACK LINK

A reliable feedback link is crucial to support real-time adaptation. Potential failures in the feedback link lead to failures in the forward link as well. In fact, if an acknowledged packet containing feedback information is lost, the subsequent transmission on the forward link is also likely to fail because of inconsistency between the physical layer configuration of the transmitter and the receiver. To deal with this problem, we propose and implement a robust wireless feedback link based on a B-CSS modulation scheme, which is known to be resilient against the severe multipath and Doppler effects that characterize the UW-A channel. Chirp signals have been presented in

the UW-A communications literature as highly reliable but low data rate alternatives [35]; they match well the requirements of feedback links, which need to be reliable but do not usually require high data rates. In addition, the B-CSS signaling scheme offers a low complexity correlation-based receiver architecture with a simple detection scheme. To the best of our knowledge, this paper is the first to propose and test the use of chirp signals for feedback links in UW-A communications.

A chirp signal is characterized by a time-varying instantaneous frequency, which changes in time from an initial value f_0 to a final value f_1. In the time domain, the signal can be expressed as

$$c(t) = \begin{cases} A\cos(2\pi f_0 t + \pi \mu t^2), & 0 \le t \le T_c \\ 0, & \text{otherwise} \end{cases} \quad (4)$$

where A is the amplitude of the chirp, f_0 is the initial chirp frequency, $\mu = \frac{f_1 - f_0}{T_c}$ is the chirp frequency-variation rate, and T_c represents the chirp period. We refer to a chirp with parameter $\mu > 0$ as an up-chirp; otherwise, we call it a down-chirp. Up and down chirp signals are almost orthogonal to each other. The total bandwidth of the chirp signal can be obtained as $B = f_1 - f_0$.

In the feedback link, we leverage the quasi-orthogonality of up and down-chirps by encoding a '1' bit with an up-chirp and a '0' bit with a down-chirp. At the receiver, two parallel correlation filters with an up and down-chirp, respectively, are used for decoding the incoming feedback packets. For each feedback bit period, one of the two correlation filters outputs a higher correlation peak, revealing the bit that was transmitted ('1' or '0'). Both transmitter and receiver functionalities of the feedback link are implemented in GNU Radio with custom C++ communication building blocks. Block diagrams of the feedback receiver and transmitter are illustrated in Fig. 4 and Fig. 5, respectively.

V. PERFORMANCE EVALUATION

In this section, we present four different sets of experiments to showcase the capabilities of our SDAM prototype. In the first two sets of experiments that are conducted in a water tank and a lake environment, we focus on demonstrating real-time implementation of OFDM physical layer parameter adaptation and switching between different communication technologies. In the third set of experiments that is conducted in a water tank, we evaluate the performance of the chirp-based feedback link. The final set of experiments, conducted in the lake, demonstrates the high-rate capabilities of the proposed SDAM.

A. TANK TESTS: PART I

We conducted experiments in a water test tank of dimensions 8 ft × 2.5 ft × 2 ft. First, we evaluated the BER performance of the implemented ZP-OFDM scheme with respect to the input SINR by varying (i) the number of subcarriers, (ii) the modulation scheme, and (iii) the error-correction coding rate. We generated OFDM signals that occupy a bandwidth of $B = 24$ kHz around a carrier frequency $f_c = 100$ kHz. We selected the operating frequency band that results in the highest transmit/receive gain for our modem by considering the combined frequency response of the transducer and the amplifiers. We defined a guard time $T_g = 15$ ms for each OFDM symbol and used $K = 128$, 256, 512, and 1024 subcarriers with either BPSK or QPSK modulation and rate $1/2$ convolutional error-correction codes.

Figure 6(a)-(b) show the BER performance versus SINR for different number of subcarriers and different modulation schemes such as BPSK and QPSK. We observe that setups with higher number of subcarriers have better BER performance. The underwater tank channel has an excessive number of channel taps (in the order of 300) with a long multipath spread and only few time variations (slow fading). In Fig. 7, we observe that for fixed total bandwidth and fixed percentage of subcarriers allocated for piloting purposes, the more the number of subcarriers the higher the number of pilot subcarriers and the better the channel estimation/resolution. Additionally, for fixed total bandwidth, the larger the number of subcarriers, the smaller the bandwidth allocated per subcarrier. As a result, the bandwidth allocated per subcarrier is considered to be within the channel coherence bandwidth and thus channel fading per subcarrier can be assumed flat.

1) ADAPTIVE CODING AND MODULATION

We fixed the number of subcarriers to $K = 1024$ and implemented an adaptive coding and modulation scheme to showcase the real-time PHY adaptation capabilities of the proposed system. We first conducted a series of experiments with different modulation schemes (i.e., $M = 2$ for BPSK and $M = 4$ for QPSK) and error-correction coding rates (i.e., no coding, $C = 1/2$). Figure 6(c) illustrates the BER performance versus SINR for different combinations of modulations and coding schemes. As expected, at low SINR, lower-data rate modulation schemes, e.g., BPSK, have better BER performance as compared to higher data rate modulation schemes, e.g., QPSK. The dashed line in Fig. 6(c) indicates a BER threshold at 5×10^{-2}, which was selected as the minimum BER requirement for this set of experiments. Thus, according to the SINR estimated at the receiver, the decision algorithm adaptively selected M and C to maximize the data rate while satisfying the BER threshold requirement.

We verified the effectiveness of real-time adaptation by comparing data rate and BER results of an adaptive scheme with a fixed/non-adaptive scheme as a function of the estimated SINR. We consider ZP-OFDM packet transmissions with $N = 16$ OFDM symbols per packet. Figure 8 shows a snapshot of experimental data recordings, where ZP-OFDM packets from index 1 to 8 demonstrate relatively lower receive SINR, compared to the packets from index 9 to 16. Figure 8 compares the performance of both fixed/non-adaptive and adaptive modulation and coding schemes in terms of data rate and BER.

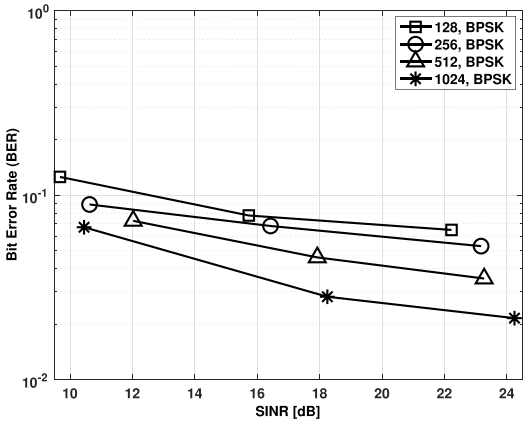

(a)

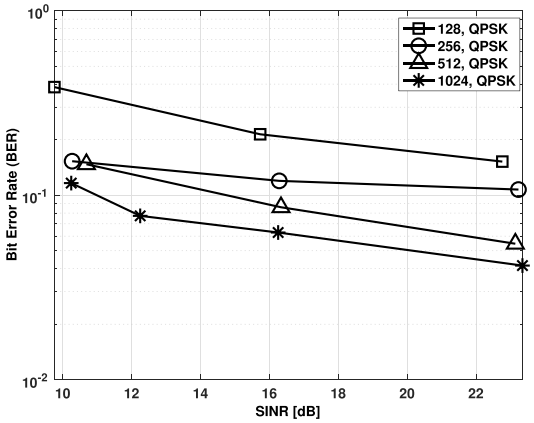

(b)

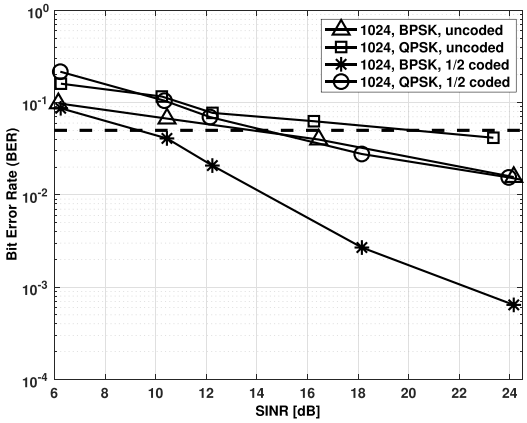

(c)

FIGURE 6. BER versus SINR for different numbers of subcarriers and encoding strategies (Tank tests: Part I). (a) BER versus SINR for BPSK modulation and $K = 128$, 256, 512, and 1024 subcarriers. (b) BER versus SINR for QPSK modulation and $K = 128$, 256, 512, and 1024 subcarriers. (c) BER versus SINR for $K = 1024$ subcarriers, different modulation and error-correction coding.

Particularly, in both experiments, software-defined underwater acoustic modems started their transmissions with the highest possible data rate (i.e., uncoded QPSK modulation). In the second packet transmission, the adaptation mechanism updated the modulation type and error-correction code and

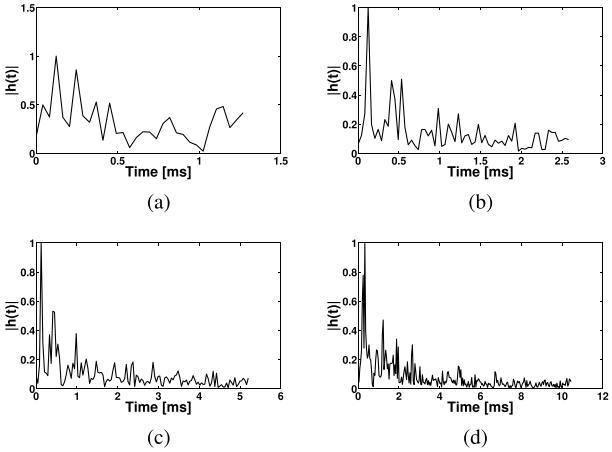

(a) (b) (c) (d)

FIGURE 7. Channel estimation for different numbers of subcarriers (Tank tests: Part I). (a) K = 128. (b) K = 256. (c) K = 512. (d) $K = 1024$.

chose a lower data rate to satisfy the BER threshold requirements of 5×10^{-2}. These choices were maintained for as long as the packet SINR profile remained constant (e.g., between 2nd and 8th packet). The adaptation decision was taken at the receiver node and communicated back to the transmitter through the chirp-based wireless feedback link. However, the fixed/non-adaptive scheme kept transmitting at the same high data rate which resulted in higher BER than the pre-defined BER threshold. At the transmission of the 9th packet the power increased (as seen also in the SINR estimation subplot of Fig. 8). Since the SINR estimates were now higher for the 9th packet transmission, the adaptive scheme chose a higher data rate for the next (i.e., 10th) packet transmission that still satisfied the BER threshold requirement. Similar adaptation would have taken place if the changes of the packet SINR profile were due to the presence of multiuser interference or heavy impulsive noise. The proposed SDAM would have adapted either its modulation scheme or its error-correction coding rate (or both) to satisfy the pre-defined BER performance requirements.

A series of experiments was conducted in Lake La Salle in Amherst, New York, which has an approximate depth of 2.33 m (7.64 ft). Two SDAM prototypes were deployed by exploiting RF cables of length 152 m (500 ft) that were connecting underwater acoustic transducers, deployed in the locations depicted in Fig. 9(b)-(c). The rest of the SDAM prototype components such as power generators, power amplifiers, voltage preamplifiers, electronic switches, and USRP N210s (Fig. 9(a)) were positioned in Baird Point (Fig. 9(c)). The underwater transducers were deployed 98 m (322 ft) apart from each other, as shown in Fig. 9(b)-(c), where they swang freely connected to their cable under the red buoys. The buoys were anchored to the bottom of the lake. In these outdoor experiments, the same parameter configuration as in the indoor test tank was used, i.e., OFDM signals of $B = 24$ kHz at carrier frequency $f_c = 100$ kHz, $K = 1024$ subcarriers, BPSK or QPSK modulation, and rate $1/2$ convolutional error-correction codes.

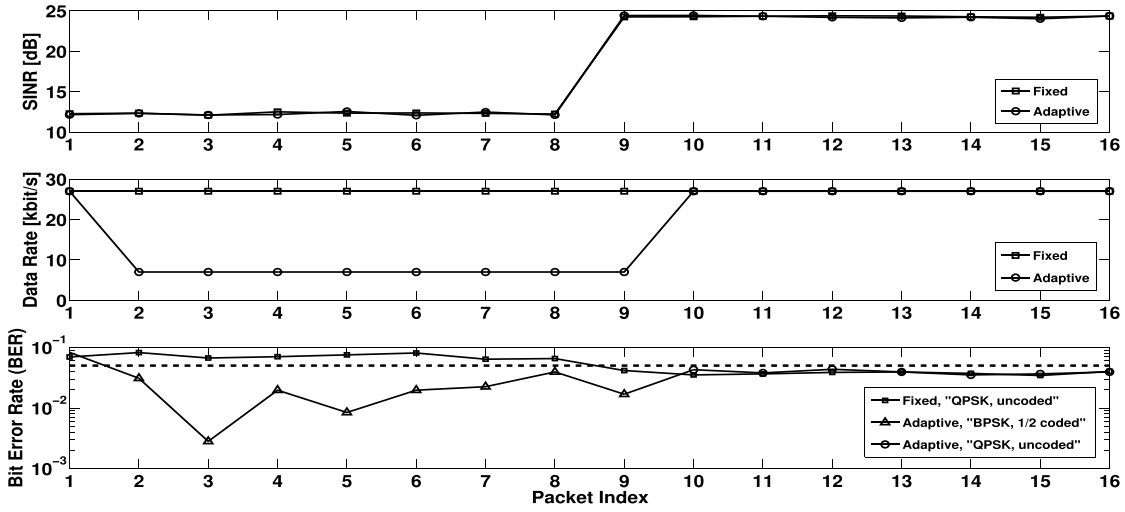

FIGURE 8. Comparison of adaptive with fixed/non-adaptive scheme in terms of SINR, data rate, and BER (Tank tests: Part I).

(a) (b) (c)

FIGURE 9. Experimental setup in Lake La Salle (Lake tests: Parts I & II). (a) Testbed setup located at Baird Point (Lake La Salle) using 152 m (500 ft) RF cables to drive each underwater transducer. (b) Underwater transducers are held by the red buoys and deployed 98 m (322 ft) apart. (c) Experimental setup in Google maps.

B. LAKE TESTS: PART I

In Fig. 10, we observe that BER performance is significantly improved (especially for high SINR) when compared to the system performance in the test tank (Fig. 6(c)), mainly due to less severe multipath. Figure 11 illustrates 10 different realizations of channel estimates from independent experiments. Although we observe that only one distinct and strong path is present, there is yet a time-varying multipath effect that cannot be neglected because of the shallow depth of the lake.

1) ADAPTIVE CODING AND MODULATION

The real-time adaptation capabilities of the proposed modem were tested in the lake environment by comparing the data rate and BER performance of an adaptive modulation/coding scheme with a fixed/non-adaptive modulation/coding scheme as a function of the estimated SINR. For this set of experiments we set the BER threshold to 10^{-3} (dashed line in Fig. 10). Figure 12 depicts a snapshot of experimental recordings, which include 21 ZP-OFDM packets.

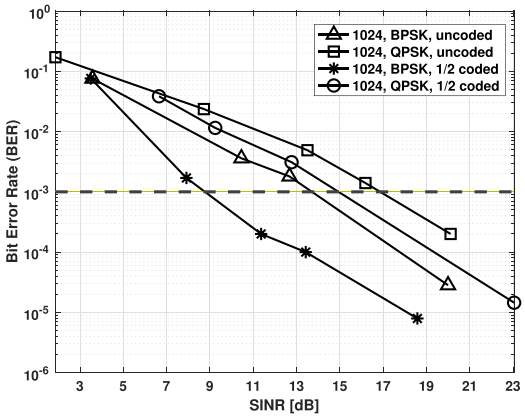

FIGURE 10. BER versus SINR for $K = 1024$ subcarriers, different modulation and error-correction coding (Lake tests: Part I).

We consider $N = 16$ OFDM symbols per packet, while receive SINR profiles vary between 10 and 20 dB for both fixed and adaptive schemes.

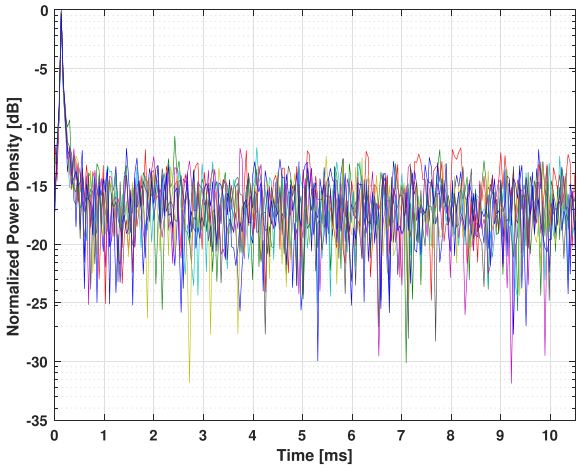

FIGURE 11. Channel estimates from 10 different ZP-OFDM packets (Lake tests: Part I).

Both types of experiments, fixed and adaptive, started with the combination of modulation and coding schemes that resulted in maximum data rate, i.e., QPSK uncoded. For the fixed/non-adaptive scheme, the data rate was maintained at its maximum value for all 21 packets. However, the BER requirement was violated from the 4th up to the 17th packet and the system performance became obsolete. More specifically, the BER requirement was violated when packets with SINR lower than 20 dB were received. Instead, in the adaptive modulation/coding mode, the data rate was adjusted following low SINR measurements at the receiver (i.e., <20 dB) to satisfy the pre-defined BER threshold requirement. In particular, modulation was changed from QPSK to BPSK as soon as the BER increased to $\sim 2.10^{-3}$ and $1/2$ rate error-correction code was used up to the 11th packet transmission. SINR profile changed into higher values from packet 11 to 17. Therefore, the mode changed into BPSK with no error-correction coding to compensate for the data rate loss. After packet 17, SINR values returned to the initial level of 20 dB, and the QPSK uncoded modulation scheme was again selected.

2) CHIRP-BASED FEEDBACK

Figure 13 depicts one of the received feedback packets that consists of two down and one up chirps. A bank of up/down chirp correlation filters at the receiver (Fig. 4) and peak detectors were used for decoding the received feedback signals. The decision block in Fig. 4 outputs '0' if correlation with a down chirp results in a higher peak, otherwise it outputs '1'. The outputs of both correlation filters are depicted in Fig. 13. We observe that the decoded feedback packet in Fig. 13 corresponds to transmitted bits '010'. The format of the feedback packet used in our experiments assigned the first bit to decide upon switching between the two available communication technologies (OFDM, DS-SS), while the other two bits were used to select between BPSK, QPSK and coded or uncoded modulation in OFDM transmissions.

3) SWITCH BETWEEN OFDM AND DS-SS

Switching between DS-SS and OFDM technologies is illustrated in Fig. 14. During this set of lake experiments, we were able to seamlessly switch between transmissions of OFDM packets (BPSK uncoded modulation, $K = 1024$ subcarriers) and spread-spectrum packets (BPSK uncoded modulation, chip length $L = 31$), both of bandwidth $B = 24$ kHz at carrier frequency $f_c = 100$ kHz.

The proposed SDAM was customized to initially transmit OFDM packets. Upon successful reception of an OFDM/DS-SS packet, feedback for switching to DS-SS/OFDM packets was sent by the receiver. In Fig. 14, we selected two different instances of an 8 s time window and focused on the received baseband signal. The bottom right part of Fig. 14 zooms in the received preamble part of the DS-SS packet (consisting of unmodulated bits) and clearly reveals the periodic pattern of the length-L spreading code. Instead, the bottom left part of Fig. 14 depicts the ZP-OFDM packet.

C. TANK TESTS: PART II

We conducted a series of experiments with a setup similar to the tank experiments presented in Section V-A. We mainly aimed to showcase the performance of the chirp-based feedback channel and provide quantitative performance evaluation of its robustness. We used B-CSS signals with varying chirp signal durations over a bandwidth $B = 97.6$ kHz around carrier frequency $f_c = 125$ kHz. Specifically, we used chirp signals with duration of $T_c = 2$ ms, $T_c = 1$ ms, $T_c = 0.5$ ms, and $T_c = 0.25$ ms, which provide data rates of 500 bit/s, 1 kbit/s, 2 kbit/s, and 4 kbit/s, respectively.

Figure 15 shows BER versus SINR performance results for different chirp signal durations. We observe that chirp signals with longer duration offer better BER performance at the expense of lower data rates. Therefore, we trade-off between robustness and data rate based on how fast or reliable we want to perform reconfiguration.

D. LAKE TESTS: PART II

A series of experiments with a setup similar to the lake experiments presented in Section V-B took place in Lake La Salle in Amherst, New York. However, in this second series of lake experiments, we demonstrated the high data rate transmission capabilities of the SDAM prototype. To that end, we used OFDM signals with $B = 97.6$ kHz around carrier frequency $f_c = 125$kHz, and $K = 8192$ subcarriers. For every data subcarrier, we tested the following modulation schemes: (i) BPSK, (ii) QAM, (iii) 8-QAM, (iv) 16-QAM, and (iv) 32-QAM with different convolutional error-correction coding rates (i.e., $1/2$, $3/4$, $7/8$).

In this set of lake experiments, to satisfy the data rate requirements of video streaming applications, we consider the overhead of preamble and pause interval durations by

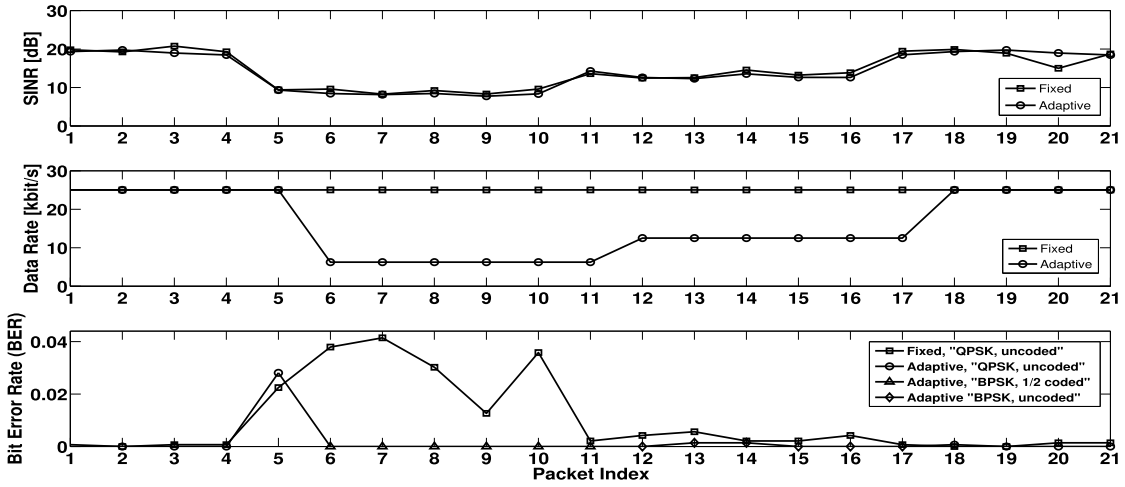

FIGURE 12. Comparison of adaptive with fixed/non-adaptive scheme in terms of SINR, data rate, and BER (Lake tests: Part I).

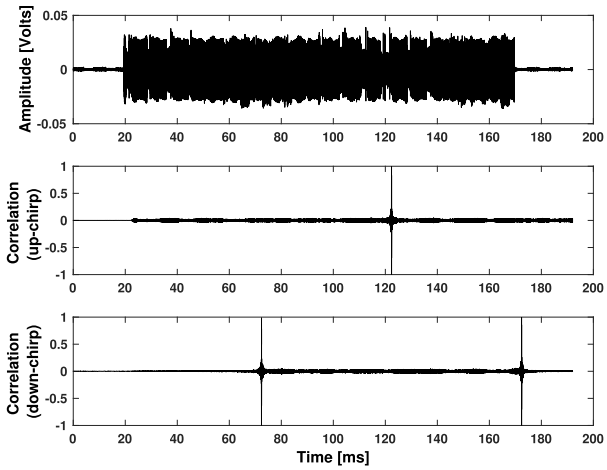

FIGURE 13. B-CSS feedback representing information bits '010' and the respective correlations with up and down chirps.

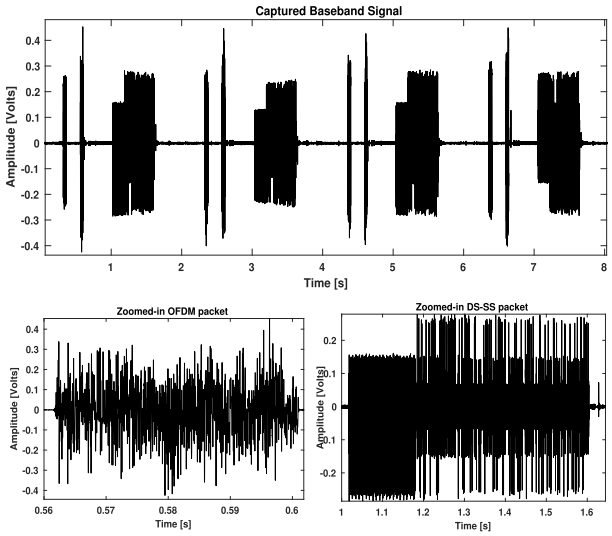

FIGURE 14. Received baseband signal consisting of OFDM and DS-SS packets.

defining data rate as follows

$$R(M, C) = \frac{NK_D C log_2(M)}{T_{pre} + T_{pau} + N(T_s + T_g)}, \tag{5}$$

where N is the number of OFDM symbols per packet, T_{pre} is the preamble duration, and T_{pau} is the pause interval duration. This is important, as all the reported data rates are obtained by real-time processing at the proposed SDAM, thus satisfying the timing deadlines required by video streaming applications.

Figure 16(a) illustrates BER versus SINR performance results for different uncoded modulation schemes, with varying data rates from 52 kbit/s to 260 kbit/s. We observe that the proposed SDAM prototype can support data rates up to 208 kbit/s at BER close to 10^{-3} and data rates up to 260 kbit/s at BER close to 10^{-2} with no FEC. In Fig. 16(b), we repeat the same experiments by superimposing channel error-correction codes with varying rates for selected modulation schemes. We observe that for low SINR values,

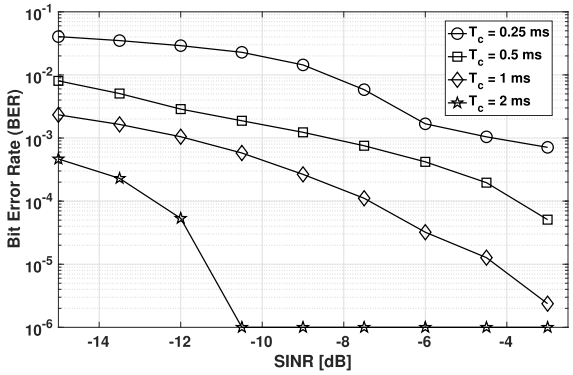

FIGURE 15. BER performance results of the B-CSS with different duration of chirp signals (Tank tests: Part II).

FEC does not improve the BER performance. However, for relatively high SINR values (e.g., 25 dB), FEC enhances the BER performance at the expense of lower data rates. As a

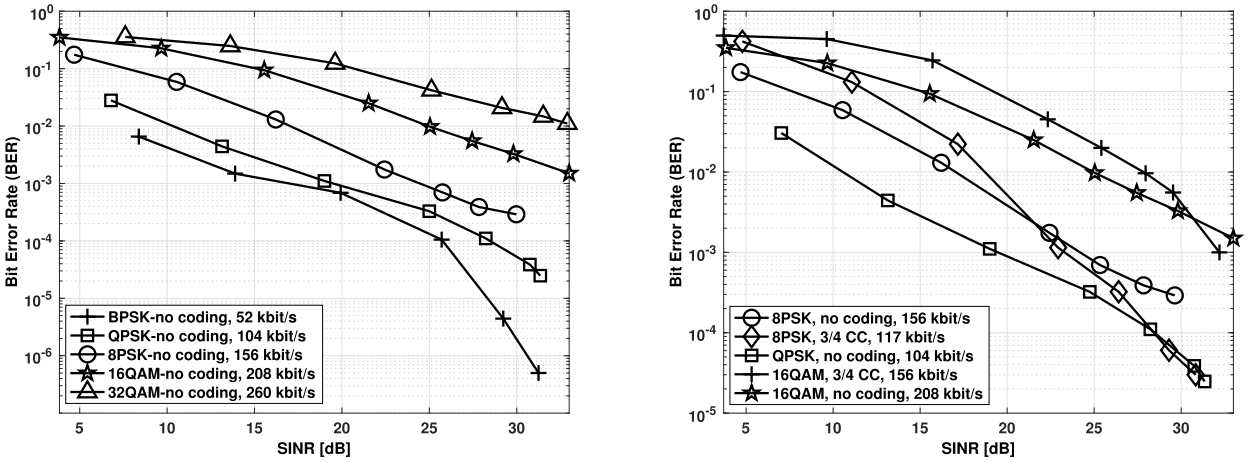

(a) (b)

FIGURE 16. BER performance results for different modulation and FEC schemes (Lake tests: Part II). (a) BER versus SINR for different modulation schemes. (b) BER versus SINR for selected modulation and FEC schemes.

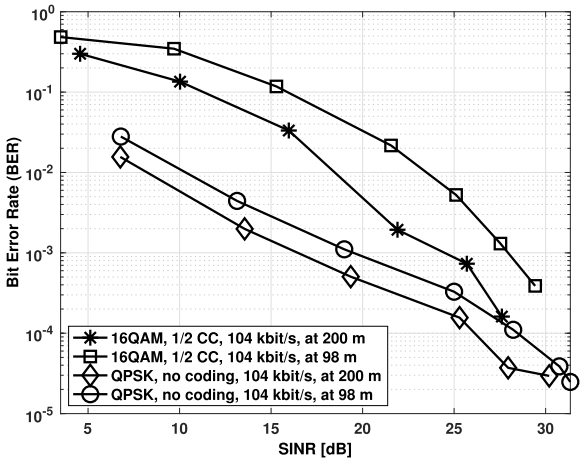

FIGURE 17. BER performance results for selected modulation and FEC schemes at different distances (Lake tests: Part II).

result, by using rate-efficient convolutional codes we can trade off BER performance for data rate, especially for higher SINR values.

Similar to our previous observation in Section V-B, the severe multipath effect, caused by the shallow water of the lake, is the main limiting factor of the BER performance of the proposed SDAM prototype. To that end, we increased the separation between the two deployed SDAM prototypes from 98 m (322 ft) to 200 m (656 ft). As a result, the number of bottom and surface reflections experienced by the paths other than line-of-sight increased, and accordingly, the effect of the multipath decreased. This acoustical phenomenon is called mode stripping effect. Figure 17 illustrates a comparison of BER versus SINR for selected pairs of modulation schemes and FEC rates over different distances. We observe that there is significant improvement in BER performance when the distance between the SDAMs increased, and the effect of multipath became less severe. Thus, we anticipate that the BER performance of the proposed SDAM prototype will improve notably in deeper underwater channels.

VI. CONCLUSIONS

We designed and built a high-rate, highly reconfigurable, software-defined underwater acoustic modem with real-time adaptation capabilities for UW-A communications. We demonstrated that the proposed SDAM prototype can support sufficiently high data rates to enable real-time video streaming applications in UW-A channels.

In addition, we introduced physical-layer adaptation mechanisms that enable real-time adaptation and optimization of the SDAM based on the environmental conditions and guarantee functionality and optimal performance at all times. More specifically, we experimentally tested the SDAM prototype both in a water test tank and a shallow lake environment and reached real-time data rates of 104 kbit/s with BER of 2×10^{-5}, 208 kbit/s with BER of 10^{-3}, and 260 kbit/s with BER of 10^{-2} at a distance of 200 m (656 ft). Furthermore, we demonstrated the flexibility of the SDAM through (i) PHY parameter adaptation in OFDM technology and (ii) seamless switching between OFDM and DS-SS communication technologies. Finally, we designed and implemented a robust chirp-based feedback link that supported wireless feedback communication and enabled real-time adaptation of the forward link to the time-varying UW-A channel characteristics and interference conditions.

ACKNOWLEDGMENT

A preliminary shorter version of this paper appeared in the Proceedings of ACM Conference on Underwater Networks & Systems (WUWNet) 2014.

REFERENCES

[1] E. Demirors, G. Sklivanitis, G. E. Santagati, T. Melodia, and S. N. Batalama, "Design of a software-defined underwater acoustic modem with real-time physical layer adaptation capabilities," in *Proc. ACM Int. Conf. Underwater Netw. Syst. (WUWNet)*, Rome, Italy, Nov. 2014, p. 25.

[2] T. Melodia, H. Kulhandjian, L.-C. Kuo, and E. Demirors, "Advances in underwater acoustic networking," in *Mobile Ad Hoc Networking: Cutting Edge Directions*, S. Basagni, M. Conti, S. Giordano, and I. Stojmenovic, Eds., 2nd ed. Hoboken, NJ, USA: Wiley, 2013, pp. 804–852.
[3] DSPComm. (2016). *AquaComm: Underwater Wireless Modem*. [Online]. Available: http://www.dspcomm.com
[4] (2016). *AquaSENT Acoustic Modems*. [Online]. Available: http://www.aquasent.com
[5] (2016). *Teledyne Benthos Acoustic Modems*. [Online]. Available: https://teledynebenthos.com
[6] (2016). *Linkquest*. [Online]. Available: http://www.link-quest.com
[7] (2016). *Evologics Underwater Acoustic Modems*. [Online]. Available: https://www.evologics.de
[8] E. Demirors, G. Sklivanitis, T. Melodia, and S. N. Batalama, "RcUBe: Real-time reconfigurable radio framework with self-optimization capabilities," in *Proc. IEEE Int. Conf. Sens., Commun., Netw. (SECON)*, Seattle, WA, USA, Jun. 2015, pp. 28–32.
[9] G. Sklivanitis, A. Gannon, S. N. Batalama, and D. A. Pados, "Addressing next-generation wireless challenges with commercial software-defined radio platforms," *IEEE Commun. Mag.*, vol. 54, no. 1, pp. 59–67, Jan. 2016.
[10] G. Sklivanitis, E. Demirors, A. M. Gannon, S. N. Batalama, D. A. Pados, and S. N. Batalama, "All-spectrum cognitive channelization around narrowband and wideband primary stations," in *Proc. IEEE Global Commun. Conf. (GLOBECOM)*, San Diego, CA, USA, Dec. 2015, pp. 1–7.
[11] G. Sklivanitis, E. Demirors, S. N. Batalama, D. A. Pados, and T. Melodia, "ROCH: Software-defined radio toolbox for experimental evaluation of all-spectrum cognitive networking," in *Proc. ACM Workshop Softw. Radio Implement. Forum (SRIF)*, Paris, France, Sep. 2015, pp. 1–10.
[12] G. Nychis, T. Hottelier, Z. Yang, S. Seshan, and P. Steenkiste, "Enabling MAC protocol implementations on software-defined radios," in *Proc. 6th USENIX Symp. Netw. Syst. Design Implement. (NSDI)*, 2009, pp. 91–105.
[13] B. Bloessl, M. Segata, C. Sommer, and F. Dressler, "An IEEE 802.11a/g/p OFDM receiver for GNU radio," in *Proc. 2nd Workshop Softw. Radio Implement. Forum (SRIF)*, New York, NY, USA, 2013, pp. 9–16.
[14] E. M. Sözer and M. Stojanovic, "Reconfigurable acoustic modem for underwater sensor networks," in *Proc. ACM Int. Workshop Underwater Netw. (WUWNet)*, Los Angeles, CA, USA, Sep. 2006, pp. 101–104.
[15] T. Fu, D. Doonan, C. Utley, R. Iltis, R. Kastner, and H. Lee, "Design and development of a software-defined underwater acoustic modem for sensor networks for environmental and ecological research," in *Proc. OCEANS*, Sep. 2006, pp. 1–6.
[16] E. Jones, "The application of software radio techniques to underwater acoustic communications," in *Proc. IEEE OCEANS*, Aberdeen, U.K., Jun. 2007, pp. 1–6.
[17] E. Demirors, G. Sklivanitis, T. Melodia, S. N. Batalama, and D. A. Pados, "Software-defined underwater acoustic networks: Toward a high-rate real-time reconfigurable modem," *IEEE Commun. Mag.*, vol. 53, no. 11, pp. 64–71, Nov. 2015.
[18] A. Radosevic, T. M. Duman, J. G. Proakis, and M. Stojanovic, "Adaptive OFDM for underwater acoustic channels with limited feedback," in *Proc. Signals, Syst. Comput. (ASILOMAR)*, Nov. 2011, pp. 975–980.
[19] P. Qarabaqi and M. Stojanovic, "Adaptive power control for underwater acoustic communications," in *Proc. IEEE OCEANS*, Santander, Spain, Jun. 2011, pp. 1–7.
[20] A. Radosevic, R. Ahmed, T. M. Duman, J. G. Proakis, and M. Stojanovic, "Adaptive OFDM modulation for underwater acoustic communications: Design considerations and experimental results," *IEEE J. Ocean. Eng.*, vol. 39, no. 2, pp. 357–370, Apr. 2014.
[21] L. Wan *et al.*, "Field tests of adaptive modulation and coding for underwater acoustic OFDM," in *Proc. 8th ACM Int. Conf. Underwater Netw. Syst. (WUWNet)*, Kaohsiung, Taiwan, 2013, p. 35.
[22] (2015). *WHOI Micromodem*. [Online]. Available: http://acomms.whoi.edu/micro-modem/
[23] S. Roy, T. M. Duman, V. McDonald, and J. G. Proakis, "High-rate communication for underwater acoustic channels using multiple transmitters and space time coding: Receiver structures and experimental results," *IEEE J. Ocean. Eng.*, vol. 32, no. 3, pp. 663–688, Jul. 2007.
[24] N. Nowsheen, C. Benson, and M. Frater, "A high data-rate, software-defined underwater acoustic modem," in *Proc. MTS/IEEE OCEANS*, Seattle, WA, USA, Sep. 2010, pp. 1–5.
[25] C. Pelekanakis, M. Stojanovic, and L. Freitag, "High rate acoustic link for underwater video transmission," in *Proc. OCEANS*, vol. 2. Sep. 2003, pp. 1091–1097.
[26] E. Demirors, J. Shi, R. Guida, and T. Melodia, "SEANet G2: Toward a high-data-rate software-defined underwater acoustic networking platform," in *Proc. ACM Int. Conf. Underwater Netw. Syst. (WUWNet)*, Shanghai, China, Oct. 2016, pp. 1–12.
[27] D. Torres, J. Friedman, T. Schmid, M. B. Srivastava, Y. Noh, and M. Gerla, "Software-defined underwater acoustic networking platform and its applications," *Ad Hoc Netw.*, vol. 34, pp. 252–264, Nov. 2015.
[28] M. Chitre, I. Topor, and T.-B. Koay, "The UNET-2 modem—An extensible tool for underwater networking research," in *Proc. MTS/IEEE OCEANS*, Yeosu, South Korea, May 2012, pp. 1–7.
[29] H. S. Dol, P. Casari, T. van der Zwan, and R. Otnes, "Software-defined underwater acoustic modems: Historical review and the NILUS approach," *IEEE J. Ocean. Eng.*, vol. 42, no. 3, pp. 722–737, Jul. 2017.
[30] E. Demirors, B. G. Shankar, G. E. Santagati, and T. Melodia, "SEANet: A software-defined acoustic networking framework for reconfigurable underwater networking," in *Proc. ACM Int. Conf. Underwater Netw. Syst. (WUWNet)*, Washington, DC, USA, Nov. 2015, p. 11.
[31] K. R. Chowdhury and T. Melodia, "Platforms and testbeds for experimental evaluation of cognitive ad hoc networks," *IEEE Commun. Mag.*, vol. 48, no. 9, pp. 96–104, Sep. 2010.
[32] S. Zhou and Z.-H. Wang, *OFDM for Underwater Acoustic Communications*. Hoboken, NJ, USA: Wiley, 2014.
[33] B. Li, S. Zhou, M. Stojanovic, L. Freitag, and P. Willett, "Multicarrier communication over underwater acoustic channels with nonuniform Doppler shifts," *IEEE J. Ocean. Eng.*, vol. 33, no. 2, pp. 198–209, Apr. 2008.
[34] G. Sklivanitis, E. Demirors, S. N. Batalama, T. Melodia, and D. A. Pados, "Receiver configuration and testbed development for underwater cognitive channelization," in *Proc. IEEE Asilomar Conf. Signals, Syst., Comput.*, Pacific Grove, CA, USA, Nov. 2014, pp. 1594–1598.
[35] L. R. LeBlanc, M. Singer, P.-P. Beaujean, C. Boubli, and J. R. Alleyne, "Improved chirp FSK modem for high reliability communications in shallow water," in *Proc. MTS/IEEE OCEANS*, Sep. 2000, pp. 601–603.

EMRECAN DEMIRORS (S'11–M'17) received the B.S. degree in electrical and electronics engineering from Bilkent University, Ankara, Turkey, in 2009, the M.S. degree in electrical engineering from the State University of New York at Buffalo, NY, USA, in 2014, and the Ph.D. degree in electrical and computer engineering from Northeastern University, Boston, MA, USA, in 2017. He is currently a Post-Doctoral Research Associate with the Department of Electrical and Computer Engineering, Northeastern University. His research interests include underwater acoustic communications and networks, Internet-of-Things, software-defined wireless communications and networks, cognitive radio networks, and body-area networks. In 2014, he was a recipient of the Nutaq Software-Defined Radio Academic US National Contest, in 2015 the Best Paper Award, and the Best Demo Second Award at the 10th ACM International Conference on Underwater Networks and Systems. He was also a recipient of the 2016 Northeastern University College of Engineering Outstanding Research Assistant Award.

GEORGE SKLIVANITIS (S'11–M'18) received the Diploma degree in electronic and computer engineering from the Technical University of Crete, Greece, in 2010, and the Ph.D. degree in electrical engineering from The State University of New York at Buffalo, in 2018. He is currently a Post-Doctoral Research Fellow with the Department of Computer and Electrical Engineering and Computer Science, Florida Atlantic University. His research interests span the areas of signal processing, software-defined wireless communications and networking, cognitive radio, and underwater acoustic communications. In 2014, he was the first finalist and was a recipient of the 2014 Nutaq Software-Defined Radio Academic U.S. National Contest and in 2015 the 10th ACM International Conference on Underwater Networks and Systems Best Demo Award. He was also a recipient of the 2015 SUNY Buffalo Graduate Student Award for Excellence in Teaching, the 2016 SUNY Buffalo Student Entrepreneur Fellowship, and the 2017 SUNY Chancellor's Award for Student Excellence.

G. ENRICO SANTAGATI (S'13) received the B.S. and M.S. degrees in telecommunication engineering from the University of Catania, Catania, Italy, in 2010 and 2012, respectively, and the Ph.D. degree in electrical and computer engineering, Northeastern University, Boston, MA, USA, in 2016. His research interests include body-area networks, acoustic and ultrasonic communications, and software-defined wireless communications. He was a recipient of the 2016 Outstanding Research Assistant Award from the Electrical and Computer Engineering Department, Northeastern University, and the Innovation Commercialization Seed Fund from the Massachusetts Technology Transfer Center.

TOMMASO MELODIA (M'07–SM'16–F'18) received the Ph.D. degree in electrical and computer engineering from the Georgia Institute of Technology, Atlanta, GA, USA, in 2007. He is currently an Associate Professor with the Department of Electrical and Computer Engineering, Northeastern University, Boston, MA, USA. He is also serving as the lead PI on multiple grants from U.S. federal agencies including the National Science Foundation, the Air Force Research Laboratory, the Office of Naval Research, and the Army Research Laboratory. He is also the Director of Research for the PAWR Project Office, a public-private partnership that is developing four city-scale platforms for advanced wireless research in the U.S. He has co-authored a paper that was recognized as the Fast Breaking Paper in the field of computer science by Thomson ISI Essential Science Indicators and a paper that received the Elsevier Top Cited Paper Award. His research focuses on modeling, optimization, and experimental evaluation of wireless networked systems, with applications to 5G networks and Internet of Things, software-defined networking, and body area networks. He was a recipient of the National Science Foundation CAREER award and of several other awards. He is the Technical Program Committee Chair for the IEEE INFOCOM 2018. He is an Associate Editor for the IEEE TRANSACTIONS ON WIRELESS COMMUNICATIONS, the IEEE TRANSACTIONS ON MOBILE COMPUTING, and the IEEE TRANSACTIONS ON BIOLOGICAL, MOLECULAR, AND MULTI-SCALE COMPUTER NETWORKS, and *Smart Health*.

STELLA N. BATALAMA (M'94–SM'15) received the Diploma degree in computer engineering and science from the University of Patras, Greece, in 1989, and the Ph.D. degree in electrical engineering from the University of Virginia, Charlottesville, VA, USA, in 1994. She is currently the Dean of the College of Engineering and Computer Science, Florida Atlantic University. From 2003 to 2004 she was the Acting Director of the Air Force Research Laboratory, Center for Integrated Transmission and Exploitation, Rome, NY, USA. From 2009 to 2011 she was the Associate Dean for research with the School of Engineering and Applied Sciences. From 2010 to 2017 she served as the Chair with the Electrical Engineering Department, The State University of New York at Buffalo. She has published over 170 papers scientific journals and conference proceedings in her research field. Her research interests include cognitive and cooperative communications and networks, multimedia security and data hiding, underwater signal processing, communications and networks. She was a recipient of the 2015 SUNY Chancellor's Award for Excellence in Research. She was an associate editor for the IEEE COMMUNICATIONS LETTERS from 2000 to 2005 and the IEEE TRANSACTIONS ON COMMUNICATIONS from 2002 to 2008.